Infrared Detection of Tropospheric Nitrogen Oxides

Haochen Zhao

Supervisor: Dr. A. Dudhia

Abstract

This paper investigates the reasons why the detection of tropospheric nitrogen oxides has never been reported via nadir-viewing instruments in infrared region. We identify regions where the concentrations of nitrogen oxides are high, and predict the infrared spectra by modifying the column atmospheric composition. Then we analyse the detection sensitivity of infrared features under different atmospheric conditions and simulate relevant concentrations from the Infrared Atmospheric Sounding Interferometer (IASI). The performance of IASI-Next Generation (IASI-NG), which is scheduled to launch by 2025, is also discussed. We conclude that the precision and noise level of current measurements do not support the detection of tropospheric nitrogen oxides, but IASI-NG has the potential to make further progress.

1. Introduction

The detection of air constituents is always an important part of atmospheric and planetary physics since it enables a deeper understanding of the Earth and climate. Among all the constituents, tropospheric nitrogen oxides are being widely studied from both physical and chemical perspectives. Nitrogen oxides (NO_x, here refers to NO and NO_2) are air pollutants that play a vital role in the tropospheric environment [1] as well as indicators of surface air quality. It largely affects the formation rate of tropospheric ozone, the abundance of hydroxyl radicals (OH) [2], and controls the efficiency with which the troposphere cleanses itself [3]. Apart from these, Filippini et al. [4] pointed out that a high level of NO_2 pollution was related to the spread of

SARS-Cov-2 infection. Shortly after, Li et al. [5] identified a significant reduction in tropospheric NO_2 which coincides with the COVID-19 lockdown period, therefore emphasising the value of NO_x as an indicator for economic, industrial, and other anthropogenic activities.

Nitrogen oxides are produced in the troposphere primarily in the form of NO. Nitric monoxide reacts rapidly with ozone to form nitrogen dioxide, which in turn is photolyzed and regenerates ozone:

$$NO + O_3 \rightarrow NO_2 + O_2\,; \qquad NO_2 + h\nu \rightarrow NO + O\,; \qquad O + O_2 + M \rightarrow O_3 + M$$

NO and NO_2 rapidly convert into each other on a time scale of minutes and are removed from the atmosphere via the formation of nitric acid (HNO_3). HNO_3 is further removed by rain or surface deposition [6]. The lifetime of NO_x is measured to vary from hours to days, depending on the region, height, time of the year, etc. The major source of nitrogen oxides is the combustion of fossil fuels. Biomass burning, microbial processes in soils and lightning are also important sources of NO_x. This is illustrated in Figure 1 [7].

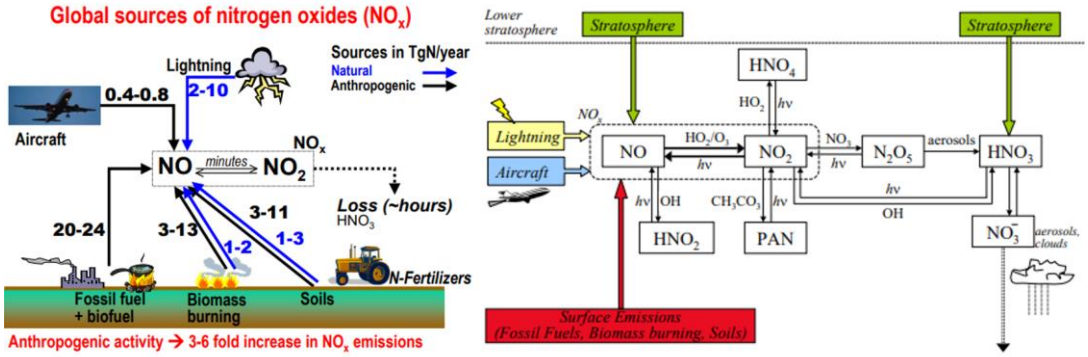

Figure 1: The major sources (left) and the life cycles (right) of tropospheric nitrogen oxides [7].

NO_x has absorption bands in the infrared and ultraviolet spectrum, which have been used for satellite measurements of NO_x concentration in the troposphere. Table 1 summarizes some previous satellites retrieving NO_x in infrared and ultraviolet region. In principle, this will also allow the detection of NO_x in the troposphere via downward-looking satellites, but no such detections have been reported. This project analyses whether tropospheric NO_x can be detected at all via downward-looking satellites in the infrared region, given that many other gases of similar concentrations have been seen. In this paper, the contribution of NO_x to the infrared spectrum is modelled, which is further used for the retrieval error analysis, and trial retrievals from IASI data are performed over identified regions of high concentrations. The predicted

Table 1: A summary of previous satellites retrieving nitrogen oxides.

	VIEWING DIRECTION	SPECTRAL COVERAGE	NO_X RETRIEVED	YEAR OF OPERATION
OMI	Downward	270-500nm	NO_2	2004~
TROPOMI [8]	Downward	270-500nm 675-775nm 2308-2380nm	NO_2	2017~
GOME [9]	Limb	240-790nm	NO_2	1995-2011
SCIAMACHY [10]	Limb	240-2380nm	NO_2	2002-2012
ACE-FTS	Limb	0.01-15μm	NO_2	2003~
MIPAS [11]	Limb	4.15-14.6μm	NO, NO_2	2002~

improvement for IASI-NG is also discussed. The results of this project will offer insights into infrared tropospheric NO_x detection and can be used as a reference for future work in this area as well as relevant retrievals from upcoming instruments.

2. Methods

2.1. Infrared Spectra

The Planck function describes the energy flux from a black body per solid angle per spectral interval at a particular temperature:

$$B_\nu(\nu, T) = \frac{2h\nu^3}{c^2} \frac{1}{e^{\frac{h\nu}{k_B T}} - 1} \tag{1}$$

Practically, the concept of brightness temperature is more frequently used for nadir-viewing satellites. The brightness temperature of an object is defined as the temperature of a black body that gives the same emission as the object at a particular frequency, and it is a measure of how strong the object radiates. Therefore, inverting the Planck function gives the frequency spectrum of brightness temperature. The molecular structure of atmospheric constituents determines how they radiates, resulting in a unique spectral feature.

What the instrument measures is the radiance L from the atmosphere and the surface, given by the radiative transfer equation:

$$L = \int_{z=0}^{\infty} B(z) d\tau(z) + B(0)\tau(0) \tag{2}$$

where the first term describes the contribution of the atmosphere at different heights, with τ being the transmittance from that height to the space, and the second term corresponds to the

contribution of the surface. Note that the spectral features vary with temperature and temperature varies with altitude. This allows us to slice through different heights in the atmosphere.

In infrared detection, the Earth surface acts as a huge emission background in its spectral region, which is better explained by rewriting the above equation as

$$L = B(T_a)(1 - \tau) + B(T_s)\tau \quad (3)$$

where the subscripts a and s represent atmosphere and surface respectively. This means that for gases near the surface the temperature contrast $|T_a - T_s|$ is small, so $B(T_a) \approx B(T_s)$ and the τ dependence cancels out, which makes them harder to be distinguished. Therefore, different surface temperatures may affect the measurements. Since the Earth surface does not radiate strongly in ultraviolet range, ultraviolet detection will not discriminate gases close to the surface and higher up.

2.2. Modelling the Spectra

The Reference Forward Model (RFM) is a general-purpose line-by-line radiative transfer model. Line-by-line means that it considers the absorption and emission properties of each individual spectral lines, enabling a complex simulation of the atmospheric spectrum. It is controlled by a driver file which the user specifies and generates the corresponding spectrum by solving the radiative transfer equation (Equation 2) [12]. In this project, the RFM is used to investigate the ν_2 and ν_3 peak of NO_2 around 750 and 1600 cm^{-1} and the NO peak around 1900 cm^{-1} at three different surface temperatures under a variety of hypothetical atmospheric conditions.

2.3. IASI

The Infrared Atmospheric Sounding Interferometer (IASI) [13] is a Fourier Transform Spectrometer carried on MetOp-A, B and C satellites, which were launched from 2006 onwards. IASI aims to provide highly accurate measurements of temperature, humidity, and atmospheric composition profiles for weather forecasting, climate monitoring, and research purposes. It is a downward-looking instrument working in the infrared region and has 8461 spectral samples in three bands between 645 and 2760 cm^{-1} with spectral sampling interval 0.25 cm^{-1} and spectral resolution 0.5 cm^{-1}. That means they cover the infrared NO_x spectral features.

The next generation of IASI instruments, IASI-NG are scheduled to launch from 2025 onwards and will contribute to atmospheric composition studies and climate research [14]. With its technological and engineering innovations, IASI-NG has half the spectral sampling interval and half the signal-to-noise ratio.

2.4. Jacobian Spectrum

The concentrations of NO_x are retrieved from measurements of the atmospheric spectrum with respect to a reference level of unit concentration. The relative uncertainty can be calculated by the Jacobian spectrum, defined as the difference in brightness temperature per unit amount of NO_x. Let $\vec{y}'$ be the measured spectrum, which contains noise with variance σ_y, and x be the concentration of NO_x. Suppose the true spectrum of the atmosphere without NO_x ($x = 0$) is given by $\vec{f}(0)$ and that with NO_x at the reference level ($x = 1$) by $\vec{f}(1)$. We can therefore define a residual spectrum $\vec{y} \equiv \vec{y}' - \vec{f}(0)$ which ideally contains only the signature of NO_x and noise, and then a Jacobian spectrum $\vec{k}$ showing the expected signature of NO_x at its reference concentration:

$$\vec{k} = \vec{f}(1) - \vec{f}(0) \approx \frac{d\vec{y}}{dx} \tag{4}$$

To retrieve the concentration we solve for x such that

$$\vec{y} = \frac{d\vec{y}}{dx} \cdot x \approx \vec{k}x \tag{5}$$

Since $\vec{y}$ and $\vec{k}$ are vectors of the same dimension and x is a scalar, for each component we have $y_i \approx k_i x_i$, which gives a series of x_i. The corresponding variance on x_i is hence $\sigma_{xi}^2 = \sigma_y^2 / k_i^2$. To emphasize the contribution of more precise points we take our retrieval as the average of x_i weighted by $1/\sigma_{xi}$. The final variance is hence

$$\frac{1}{\sigma_x^2} = \sum \frac{1}{\sigma_{xi}^2} = \frac{1}{\sigma_y^2} \sum k_i^2 \tag{6}$$

$$\sigma_x^2 = \frac{\sigma_y^2}{\sum k_i^2} = \frac{\sigma_y^2}{\vec{k} \cdot \vec{k}} \tag{7}$$

3. Detection Sensitivity

Previous work with TROPOMI suggests that high levels of NO_x can be observed in industrial areas like London, western Germany, Mexico City and East China [8]. This is as expected from our earlier discussions on Figure 1. To investigate these areas, we used the RFM to generate spectra of (a) the atmosphere excluding NO_x, (b) NO_x in clean air, which may be found in areas away from human activities, for instance the Atlantic, and (c) NO_x in polluted air, which may be found in the above industrial areas. The results are shown in Figure 2. We can see that most of the NO_x features are small compared with the spectrum of other molecules in the atmosphere, even the strongest NO_2 ν_3 peak is likely to be covered by the wide and large H_2O feature.

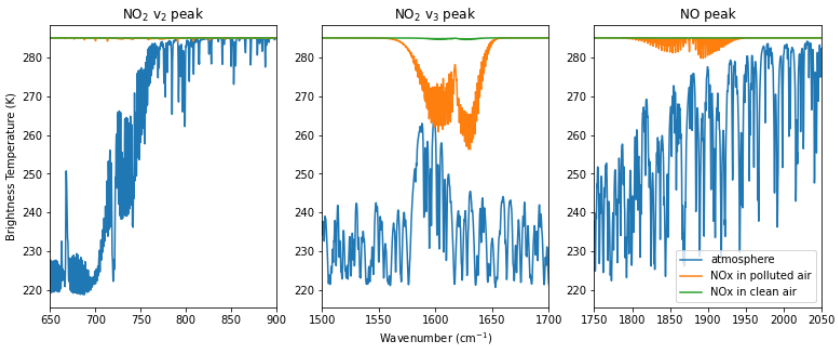

Figure 2: The comparison between the spectrum of the atmosphere excluding NO_x and of NO_x solely in clean and polluted case.

More quantitatively, since concentrations of NO_x are retrieved from IASI data, we want to simulate the uncertainties of the retrieval. A series of modified NO_x profiles are constructed, assuming that anthropogenic NO_x is mostly produced near the surface. In each modified profile, one mole of NO_x is uniformly distributed throughout a vertical column extending from the surface to different heights, above which the profile returns to the clean air level. The retrieval uncertainties can then be found from Section 2.4.

In practice, the RFM is used to simulate $\vec{f}(0)$ and $\vec{f}(1)$, with which we can calculate $\vec{k}$ and thus σ_x^2. The retrieval uncertainty is therefore found by

$$\delta u = \pm\sigma_x \cdot \int \frac{1}{Mg} v(p)dp \tag{8}$$

where M is the molar mass of air, g is gravitational acceleration and $v(p)$ is the volume mixing ratio of NO_x and the integral equals the total amount of NO_x in a vertical column.

Using the RFM, spectra of NO_x with 10 modified profiles and 3 surface temperatures are generated and the above method gives the retrieval uncertainties, as illustrated in Figure 3. The retrieval uncertainties for all three features increases as the molecules are closer to the surface, and shows a negative correlation with surface temperature. It also worth noticing that, when close to the surface, the uncertainties for NO and NO_2 ν_2 peaks are greater than 1 mol/m^2, which corresponds to more than 100% error, while for NO_2 ν_3 peak, the strongest spectral feature, the error exceeds 1000%. This means that H_2O almost completely obscures any tropospheric signal near the surface. As most of tropospheric nitrogen oxides comes from human activities on the ground, the spectral features are mostly covered by other molecules like H_2O, which explains why one may not expect to observe NO_x via nadir-viewing infrared satellites unless NO_x is redistributed to higher altitudes and becomes more detectable by convection.

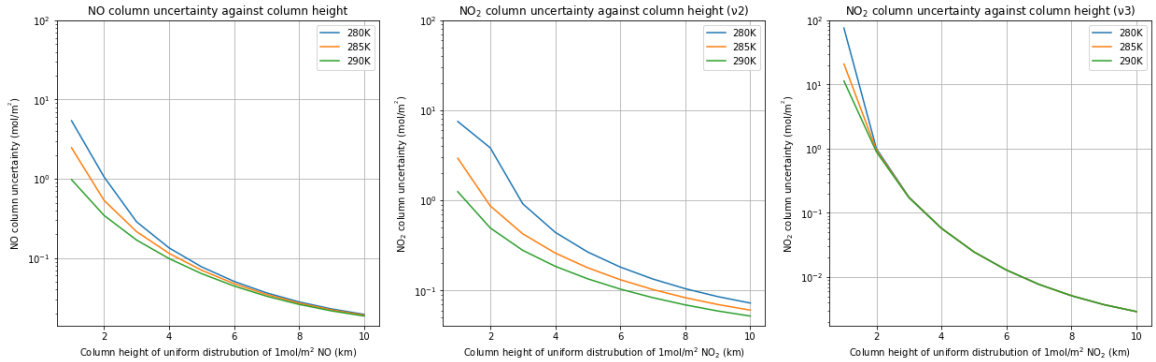

Figure 3: The retrieval uncertainties of three NO_x features with 1 mol/m^2 NO and NO_2 uniformly distributed from the ground to different heights. The colour of curves represents different surface temperatures. The atmospheric temperature at the surface is kept at 285K. Spectral sampling interval 0.25 cm^{-1} in order to simulate IASI.

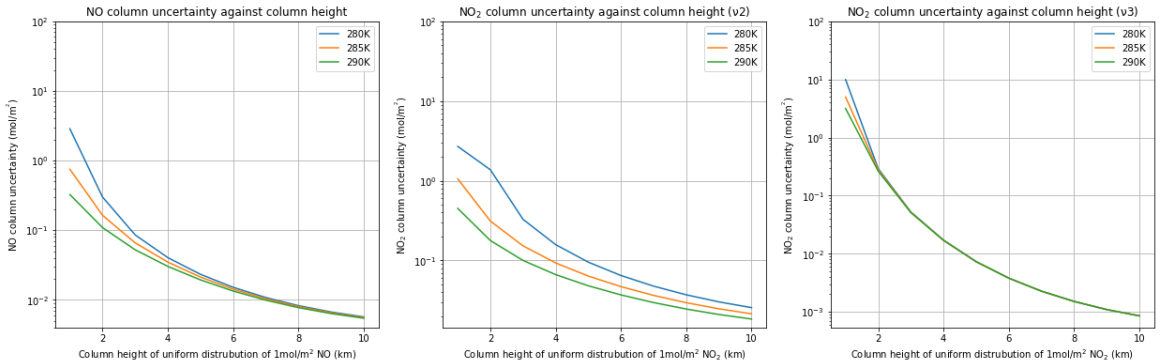

Figure 4: Retrieval uncertainties of IASI-NG for NO (left), NO_2 ν_2 (middle), and NO_2 ν_3 (right) peaks. Spectral sampling interval 0.125 cm^{-1}, half the noise from IASI, and other conditions are kept the same as in the IASI case in order to simulate IASI-NG.

Meanwhile, IASI-NG is expected to have a much better performance than the current IASI in sensing tropospheric NO_x. Similar steps as in Section 3 are carried out for IASI-NG to find its theoretical detection sensitivity, which is demonstrated in Figure 4. While the uncertainty for NO_2 ν_3 peak is still high when close to the surface, for NO and NO_2 ν_2 peaks the uncertainties drop to less than 50% at a surface temperature of 290K. This means that IASI-NG has the potential to provide more information about tropospheric NO_x.

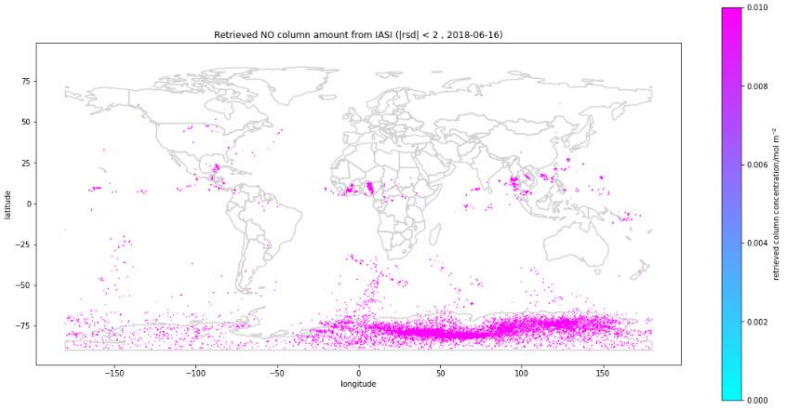

Figure 5: NO column amount retrieved from IASI. Column amount (mol/m^2) refers to the total amount of gas molecules in a vertical column and is equal to the concentration of the gas molecule integrated vertically from the ground to the top of the atmosphere. Negative column amounts are shown in blank.

4. Investigation with Real Data

Scalar linear retrieval (SLR) is an algorithm designed to detect spectral features of a particular molecule within IASI spectra [15]. It is applied for retrievals from IASI in this report. Since the surface temperature is high compared with the atmosphere in summer, a trial retrieval of NO and NO_2 ν_2 peaks from IASI is performed from 16th to 20th June 2018. As shown in Figure 5, most of the NO retrievals are negative, which makes retrievals of NO much less informative and is suspected to be resulted from a scaling algorithm in IASI. In

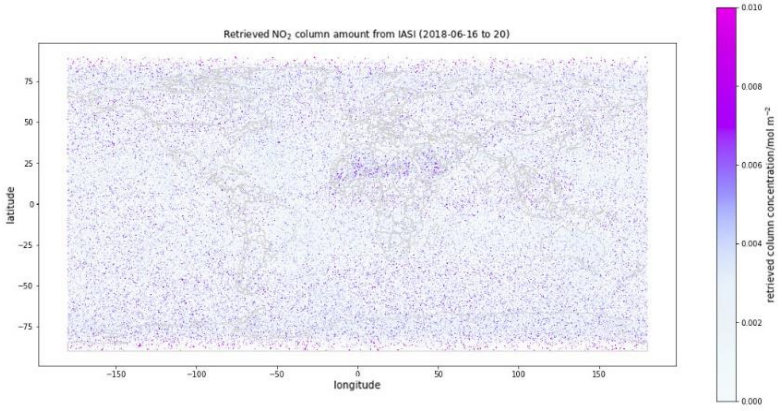

Figure 6: NO_2 column amount retrieved from IASI from 2018-06-16 to 2018-06-20. Data with large standard deviation ($\sigma >$ 2 mol/m^2) is filtered out. Only points where the standard deviation of retrieval is smaller than the retrieved column amount are plotted, so as to highlight features with certainty.

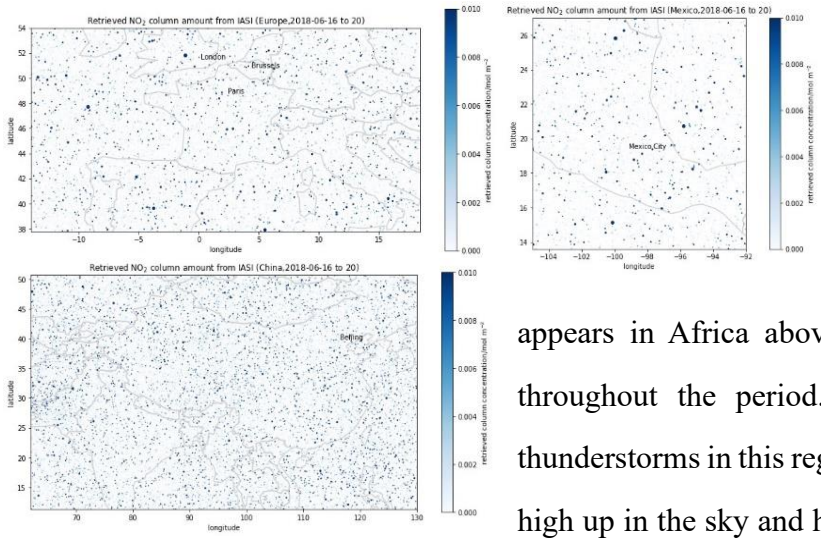

Figure 7: NO_2 retrievals over some industrial areas. 2018-06-16 to 20.

Figure 6 we can see that most of the places are covered by noise and no obvious hotspots can be identified. However, a vague NO_2 trace appears in Africa above the equator, and it persists throughout the period. This is explained by huge thunderstorms in this region, which produces NO_x from high up in the sky and hence is more likely to be seen. Previous work with OMI reports this feature as well which reassures our result [16]. Zooming in at expected hotspots like London, Mexico City and East China, as illustrated in Figure 7, no obvious signatures are observed. This agrees with our discussion in Section 3 that NO_x near the surface can hardly be detected.

5. Conclusion

We identify three different infrared absorption features of NO_x and simulate the performance of IASI and IASI-NG in detecting NO_x using each of these bands. Based on data retrieved from previous satellites, we identify areas with high levels of nitrogen oxides in the troposphere. We obtain the infrared spectra of NO_x in 10 modified atmospheric conditions at 3 surface temperatures via the RFM, which are further used to deduce the sensitivity of satellite detection on three NO_x emission features. The results show that tropospheric NO_x is harder to be observed when close to the ground. The ν_3 peak of NO_2 has the largest retrieval uncertainty while the NO and ν_2 NO_2 peaks are relatively easier to detect, although the near surface uncertainties are still greater than 100%. We also retrieve measurements from IASI and the near surface features can hardly be seen, while tropical thunderstorms are identified by a vague trace. The reason why tropospheric NO_x has not been retrieved using nadir-viewing infrared instruments is that most of the features are covered by other molecules in the atmosphere. Thus, instruments with higher sensitivity and less noise are required for nadir detection of tropospheric nitrogen oxides in infrared region. This situation is believed to be improved in the future with the help of IASI-NG.

References

[1] Jiang, Z. et al. Decadal variabilities in tropospheric nitrogen oxides over united states, europe, and china. *Journal of Geophysical Research: Atmospheres*, 127(3):e2021JD035872, 2022. e2021JD035872 2021JD035872.

[2] L. N. Lamsal, et al. Indirect validation of tropospheric nitrogen dioxide retrieved from the omi satellite instrument: Insight into the seasonal variation of nitrogen oxides at northern midlatitudes. *Journal of Geophysical Research: Atmospheres*, 115(D5), 2010.

[3] J. Bradshaw, et al. Observed distributions of nitrogen oxides in the remote free troposphere from the nasa global tropospheric experiment programs. *Reviews of Geophysics*, 38(1):61–116, 2000.

[4] Filippini, T., K. J. Rothman, A. Goffi, F. Ferrari, G. Maffeis, N. Orsini, and M. Vinceti. Satellite-detected tropospheric nitrogen dioxide and spread of sars-cov-2 infection in northern italy. *Science of The Total Environment*, 739:140278, 2020.

[5] Yun Li, Moming Li, Megan Rice, and Chaowei Yang. Impact of covid-19 containment and closure policies on tropospheric nitrogen dioxide: A global perspective. *Environment International*, 158:106887, 2022.

[6] Jennifer A. Logan. Nitrogen oxides in the troposphere: Global and regional budgets. *Journal of Geophysical Research: Oceans*, 88(C15):10785–10807, 1983.

[7] faculty.washington.edu. https://faculty.washington.edu/jaegle/558/ozone_NOx.pdf#:~:text=In%20the%20upper%20troposphere%2C%20HNO%203%20is%20recycled,the%20surface%2C%20but%201-2%20weeks%20in%20upper%20troposphere. [Accessed 16-03-2024].

[8] J. D. East, B. H. Henderson, S. L. Napelenok, S. N. Koplitz, G. Sarwar, R. Gilliam, A. Lenzen, D. Q. Tong, R. B. Pierce, and F. Garcia-Menendez. Inferring and evaluating satellite-based constraints on no_x emissions estimates in air quality simulations. *Atmospheric Chemistry and Physics*, 22(24):15981–16001, 2022.

[9] K. L. Chan, et al. Global ozone monitoring experiment-2 (gome-2) daily and monthly level-3 products of atmospheric trace gas columns. *Earth System Science Data*, 15(4):1831–1870, 2023.

[10] Randall V. Martin, C. E. Sioris, K. Chance, T. B. Ryerson, T. H. Bertram, P. J. Wooldridge, R. C. Cohen, J. Andy Neuman, A. Swanson, and Frank M. Flocke. Evaluation of space-based constraints on global nitrogen oxide emissions with regional aircraft measurements over and downwind of eastern north america. *Journal of Geophysical Research: Atmospheres*, 111(D15), 2006.

[11] C. Crevoisier. 7.11 - use of hyperspectral infrared radiances to infer atmospheric trace gases. In Shunlin Liang, editor, *Comprehensive Remote Sensing*, pages 345–387. Elsevier, Oxford, 2018.

[12] Anu Dudhia. The reference forward model (rfm). *Journal of Quantitative Spectroscopy and Radiative Transfer*, 186:243–253, 2017. Satellite Remote Sensing and Spectroscopy: Joint ACE-Odin Meeting, October 2015.

[13] About IASI — esa.int. https://www.esa.int/Applications/Observing_the_Earth/Meteorological_missions/MetOp/About_IASI. [Accessed 18-03-2024].

[14] C. Crevoisier, et al. Towards iasi-new generation (iasi-ng): impact of improved spectral resolution and radiometric noise on the retrieval of thermodynamic, chemistry and climate variables. *Atmospheric Measurement Techniques*, 7(12):4367–4385, 2014.

[15] Oxford IASI SLRs — eodg.atm.ox.ac.uk. https://eodg.atm.ox.ac.uk/IASI/slr/about.html. [Accessed 09-04-2024].

[16] E. J. Bucsela, N. A. Krotkov, E. A. Celarier, L. N. Lamsal, W. H. Swartz, P. K. Bhartia, K. F. Boersma, J. P. Veefkind, J. F. Gleason, and K. E. Pickering. A new stratospheric and tropospheric no_2 retrieval algorithm for nadir-viewing satellite instruments: applications to omi. *Atmospheric Measurement Techniques*, 6(10):2607–2626, 2013.